Monthly Notices
of the
ROYAL ASTRONOMICAL SOCIETY

MNRAS **457,** 2845–2854 (2016) doi:10.1093/mnras/stw184

Towards a census of supercompact massive galaxies in the Kilo Degree Survey

C. Tortora,[1]★ F. La Barbera,[1] N. R. Napolitano,[1] N. Roy,[1,2] M. Radovich,[3] S. Cavuoti,[1] M. Brescia,[1] G. Longo,[2] F. Getman,[1] M. Capaccioli,[2] A. Grado,[1] K. H. Kuijken,[4] J. T. A. de Jong,[4] J. P. McFarland[5] and E. Puddu[1]

[1]*INAF – Osservatorio Astronomico di Capodimonte, Salita Moiariello, 16, I-80131 Napoli, Italy*
[2]*Dipartimento di Scienze Fisiche, Università di Napoli Federico II, Compl. Univ. Monte S. Angelo, I-80126 Napoli, Italy*
[3]*INAF – Osservatorio Astronomico di Padova, Via Ekar, I-36012 Asiago VI, Italy*
[4]*Leiden Observatory, Leiden University, PO Box 9513, NL-2300 RA Leiden, the Netherlands*
[5]*Kapteyn Astronomical Institute, University of Groningen, PO Box 800, NL-9700 AV Groningen, the Netherlands*

Accepted 2016 January 20. Received 2016 January 12; in original form 2015 July 5

ABSTRACT

The abundance of compact, massive, early-type galaxies (ETGs) provides important constraints to galaxy formation scenarios. Thanks to the area covered, depth, excellent spatial resolution and seeing, the ESO Public optical Kilo Degree Survey (KiDS), carried out with the VLT Survey Telescope, offers a unique opportunity to conduct a complete census of the most compact galaxies in the Universe. This paper presents a first census of such systems from the first 156 deg^2 of KiDS. Our analysis relies on *g*-, *r*- and *i*-band effective radii (R_e), derived by fitting galaxy images with point spread function (PSF)-convolved Sérsic models, high-quality photometric redshifts, z_{phot}, estimated from machine learning techniques, and stellar masses, $M_\star$, calculated from KiDS aperture photometry. After massiveness ($M_\star \gtrsim 8 \times 10^{10}\,M_\odot$) and compactness ($R_e \lesssim 1.5$ kpc in *g*, *r* and *i* bands) criteria are applied, a visual inspection of the candidates plus near-infrared photometry from VIKING-DR1 are used to refine our sample. The final catalogue, to be spectroscopically confirmed, consists of 92 systems in the redshift range $z \sim 0.2$–0.7. This sample, which we expect to increase by a factor of 10 over the total survey area, represents the first attempt to select massive supercompact ETGs (MSCGs) in KiDS. We investigate the impact of redshift systematics in the selection, finding that this seems to be a major source of contamination in our sample. A preliminary analysis shows that MSCGs exhibit negative internal colour gradients, consistent with a passive evolution of these systems. We find that the number density of MSCGs is only mildly consistent with predictions from simulations at $z > 0.2$, while no such system is found at $z < 0.2$.

Key words: galaxies: elliptical and lenticular, cD – galaxies: evolution – galaxies: general – galaxies: structure.

1 INTRODUCTION

The understanding of the physical processes which drive the galaxy mass built up and size accretion are among the most timely topics in galaxy evolution studies. Massive early-type galaxies (ETGs) are found to be much more compact in the past than in the present Universe (Daddi et al. 2005; Trujillo et al. 2006, 2007; van der Wel et al. 2008). At redshifts $z > 2$, while the massive star-forming discs have effective radii of several kpc (Genzel et al. 2008), the quenched spheroids ('red nuggets') have small effective radii of about 1 kpc. Such red nuggets are thought to form through a chain of different processes: (a) accretion-driven violent disc instability, (b) dissipative contraction resulting in the formation of compact, star-forming 'blue nuggets', (c) quenching of star formation (Dekel & Burkert 2014). After these processes occur, a gradual expansion in size of the red nuggets may take place, leading to the formation of the massive ETGs we observe in the nearby Universe. Theoretical studies point to dry mergers as the dominant mechanism for the size and stellar mass growth of very dense massive galaxies (Khochfar & Silk 2006). In particular, minor mergers would provide a modest stellar mass accretion, but a strong evolution in galaxy size (van

★ E-mail: ctortora@na.astro.it

Dokkum et al. 2010; Hilz, Naab & Ostriker 2013; Belli, Newman & Ellis 2014; Tortora et al. 2014). Mergers are believed to be common for very massive systems at high redshifts, with major merger rates (mergers per galaxy per Gyr) in the range 0.3–1 Gyr^{-1} at $z \sim 2$ and smaller than 0.2 Gyr^{-1} at $z \lesssim 0.5$ (Hopkins et al. 2010). An alternative scenario explains the size evolution as the result of (e.g.) quasar feedback, rather than merging, making galaxies to puff up after a lost of large amounts of (cold) gas (Fan et al. 2008, 2010).

Over cosmic time, one may expect that high-z compact galaxies evolve into present-day, massive, big galaxies. However, a fraction of these objects might survive intact till the present epoch, resulting in compact, relic systems in the nearby Universe characterized by old stellar populations. Recently there have been some efforts to search for massive compact galaxies at low redshifts (Trujillo et al. 2009; Taylor et al. 2010; Valentinuzzi et al. 2010; Shih & Stockton 2011; Trujillo, Carrasco & Ferré-Mateu 2012; Damjanov et al. 2013, 2014, 2015a; Poggianti et al. 2013a,b; Saulder, van den Bosch & Mieske 2015) and investigate further their dynamical and stellar population properties, as well as the role of environment on their properties (e.g. Ferré-Mateu et al. 2012; Läsker et al. 2013; Trujillo et al. 2014; Damjanov et al. 2015b; Ferré-Mateu et al. 2015; Stringer et al. 2015; Yildirim et al. 2015; Wellons et al. 2016).

In some theoretical models, that include the effect of galaxy mergers, the fraction of massive objects that would survive without undergoing any significant transformation since $z \sim 2$ to the present could reach a fraction of about 1–10 per cent (Hopkins et al. 2009; Quilis & Trujillo 2013). At 'low' redshifts ($z \lesssim 0.2$), theoretical models predict a density of relic remnants in the range 10^{-7}–10^{-5}, which means that, in large surveys like the Sloan Digital Sky Survey (SDSS), we might expect to find a few candidates in this redshift range. However, recent observational works have shown the paucity of old, supercompact ($R_\mathrm{e} \lesssim 1.5$ kpc), massive ($M_\star \gtrsim 10^{11}\,\mathrm{M}_\odot$) galaxies in the local Universe ($z \lesssim 0.2$; Trujillo et al. 2009; Taylor et al. 2010; Ferré-Mateu et al. 2012). Indeed, NGC1277, a nearby lenticular galaxy in the Perseus cluster, is actually the only well-characterized, old system at $z \sim 0$, that might be a true relic galaxy (Trujillo et al. 2014; see also Martín-Navarro et al. 2015). Other candidates have been recently detected by Saulder et al. (2015), although only a few of them fulfill the above (restrictive) size and mass criteria ($R_\mathrm{e} \lesssim 1.5$ kpc and $M_\star \gtrsim 10^{11}\,\mathrm{M}_\odot$), none of them being at $z < 0.05$. Larger numbers of old compact systems have been found at lower masses ($<10^{11}\,\mathrm{M}_\odot$), when relaxing the compactness selection criteria (Valentinuzzi et al. 2010; Poggianti et al. 2013a). The (almost) lack of nearby supercompact, relic systems may represent a challenge for the current paradigm of galaxy formation; in particular, we have to understand whether this lack is due to some observational bias, e.g. the limited spatial resolution of photometric data at $z \sim 0$; a failure of theoretical predictions; and/or an environmental effect, for which, as suggested by NGC 1277, relic galaxies might be more frequent in high-density cluster regions.

In the intermediate-redshift range ($0.2 \lesssim z \lesssim 0.7$), compacts have been recently investigated in detail by Damjanov et al. (2014), who selected ∼200 massive compacts from a sample of stellar-like objects within the 6373.2 deg^2 of the BOSS survey; 20 per cent of these galaxies are dominated by old stellar populations, which make them reliable candidates to be the product of the unperturbed evolution of compact high-z systems. However, 93 per cent of these galaxies do not have measured R_e which hampers the selection of such systems as truly compact objects. More recently, Damjanov et al. (2015a), have analysed *F814W HST* images for the COSMOS field, providing robust size measurements for a sample of 1599 compact systems in the range $0.2 \lesssim z \lesssim 0.8$. Other studies have performed detailed analysis of stellar populations and morphology of small samples of compact galaxies at these redshifts (Hsu, Stockton & Shih 2014; Stockton et al. 2014). The population of dense passively evolving galaxies in this intermediate-redshift range possibly represents a link between compact systems, dominating the massive quiescent galaxy population at high z, and their descendants in the nearby Universe. Indeed, large samples of compacts, with high-quality photometry (to derive reliable structural parameters), and spectroscopic data, are actually necessary to better understand the formation and evolution of these systems.

The Kilo Degree Survey (KiDS; de Jong et al. 2015) is one of the ESO public surveys carried out with the VLT Survey Telescope (VST; Capaccioli & Schipani 2011) equipped with the 1 deg^2 field of view and high angular resolution (0.2 arcsec pixel^{-1}) OmegaCAM camera (Kuijken et al. 2004; Kuijken 2011). KiDS is mainly designed for weak lensing studies, providing deep imaging in four optical bands (*ugri*), over a 1500 deg^2 of the sky with excellent seeing (e.g. 0.65 deg^2 median FWHM in r band). The high image quality and deep photometry are ideal to investigate massive compact systems.

According to predictions from simulations (Guo et al. 2011a, 2013), we can expect to find ∼0.3–3.5 relic per deg^2, at redshift $z < 0.5$. This prediction does critically depend on the physical processes shaping size and mass evolution of galaxies, such as the relative importance of major and minor galaxy merging.

Several compact galaxy definitions have been adopted in the literature (Trujillo et al. 2009; Taylor et al. 2010; Poggianti et al. 2013a; Damjanov et al. 2015a). In this work, we present the properties of a sample of dense massive galaxy candidates in KiDS, defining as massive supercompact galaxies (MSCGs) those early-type systems with $M_\star > 8 \times 10^{10}\,\mathrm{M}_\odot$ and $R_\mathrm{e} < 1.5$ kpc (Trujillo et al. 2009). These selection criteria are rather conservative, providing the ideal benchmark for galaxy evolution theories. The paper is organized as follows. In Section 2 we present the KiDS data sample and the selection of our photometrically selected compact galaxies. The main results, and in particular the evolution of number density as a function of redshift, are presented in Section 3. A discussion of the results and future prospects are outlined in Section 4. We adopt a cosmological model with $(\Omega_\mathrm{m}, \Omega_\Lambda, h) = (0.3, 0.7, 0.70)$, where $h = H_0/100\,\mathrm{km\,s^{-1}\,Mpc^{-1}}$ (Komatsu et al. 2011).

2 SAMPLE SELECTION

The galaxy sample presented in this work is based on the data included in the first and second data releases of KiDS presented in de Jong et al. (2015), which we address the interested reader for details. The total data set includes 156 KiDS pointings (133 from the KiDS data release 2), in which we have identified about 22 million sources including ∼7 millions which have been classified as high-quality extended sources (mostly galaxy-like, see below). A full description of the galaxy sample is given in Napolitano et al. (in preparation). In the following section, we summarize the main steps for the galaxy selection procedure and the determination of galaxy physical quantities as structural parameters, photometric redshifts and stellar masses.

2.1 KiDS high signal-to-noise galaxy sample

We start from the KiDS multiband source catalogues, where the photometry has been obtained with SExtractor (Bertin & Arnouts 1996) in dual image mode, using as reference the positions of the

sources detected in the *r*-band images. While magnitudes are measured for all of the filters, the star/galaxy separation, positional and shape parameters are based on the *r*-band data. The choice of *r* band is motivated by the fact that it typically has the best image quality and thus provides the most reliable source positions and shapes. Critical areas as saturated pixels, star spikes, reflection haloes, satellite tracks, etc. have been masked using both a dedicated automatic procedure and visual inspection. The total area after removing the borders of the individual KiDS pointings is 163.9 deg^2, while the unmasked effective area adopted is of 105.4 deg^2.

Star/galaxy separation is based on the distribution of the SExtractor parameters CLASS_STAR and S/N (signal-to-noise ratio) of a number of sure stars (see La Barbera et al. 2008 and de Jong et al. 2015 for further details). We have further retained those sources which were marked as being out of critical area from our masking procedure. From the original catalogue, the star/galaxy separation leaves ∼11 million galaxies, of which ∼7 millions have high-quality photometry being non-deblended sources located out of the masked area.

To perform accurate surface photometry and determine reliable structural parameters, the highest quality sources have been further selected (La Barbera et al. 2008, 2010). Thus, we have finally gathered those systems with the highest S/N in the *r*-band images, $(S/N)_r \equiv 1/\mathrm{MAGERR\_AUTO\_r} > 50$ (La Barbera et al. 2008, 2010; Roy et al., in preparation). This sample consists of ∼380 000 galaxies.

Relevant properties for each galaxy are derived as described here below.

(i) *Photometry.* As a standard KiDS catalogues' parameters, we have derived SExtractor aperture photometry in the four bands (*ugri*) within several radii. For our analysis we have adopted aperture magnitudes MAGAP_2, MAGAP_4 and MAGAP_6, measured within circular apertures of 2 arcsec, 4 arcsec and 6 arcsec of diameter, respectively, while a first probe of the total magnitude is provided by the Kron-like MAG_AUTO.

(ii) *Structural parameters.* Surface photometry is performed using the 2dphot environment. 2dphot is an automatic software designed to obtain both integrated and surface photometry of galaxies in wide-field images. The software first produces a local point spread function (PSF) model from a series of identified *sure stars*. This is done, for each galaxy, by fitting the four closest stars to that galaxy with a sum of three two-dimensional Moffat functions. Then galaxy snapshots are fitted with PSF-convolved Sérsic models having elliptical isophotes plus a local background value (see La Barbera et al. 2008 for further details). The fit provides the following parameters for the four wavebands: surface brightness μ_e, circularized effective radius, R_e, Sérsic index, n, total magnitude, m_S, axis ratio, q and position angle. As it is common use in the literature, in the paper we use the circularized effective radius, R_e, defined as $R_e = \sqrt{q}R_{e,maj}$, where $R_{e,maj}$ is the major-axis effective radius.

(iii) *Photometric redshifts.* Redshifts are determined with the Multi Layer Perceptron with Quasi Newton Algorithm (MLPQNA) method (Brescia et al. 2013, 2014), and fully presented in Cavuoti et al. (2015), which we refer for all details. Both apertures of 4 arcsec and 6 arcsec of diameter are used. In machine learning supervised methods, a knowledge sample is needed to train the neural network performing the mapping between magnitudes and redshift. The knowledge base consisted on spectroscopic redshift from the SDSS data release 9 (SDSS-DR9; Ahn et al. 2012) and Galaxy And Mass Assembly data release 2 (GAMA-DR2; Driver et al. 2011) which together provide redshifts up to $z \lesssim 0.8$. This knowledge base includes ∼60 000 objects, 60 per cent of which are used as training sample, and the remaining ones are used for the blind test set. The redshifts in the blind test sample resemble the spectroscopic redshifts quite well. The scatter in the quantity $\Delta z \equiv (z_{spec} - z_{phot})/(1 + z_{spec})$ is ∼0.03. After these experiments, we have finally produced the final catalogue of redshifts for our sample. The cut operated in the fitting magnitudes to resemble the luminosity ranges in the knowledge base will impact the completeness in the faint regime. But our high-S/N sample is not affected by this source of incompleteness.

(iv) *Stellar masses.* We have used the software LE PHARE (Arnouts et al. 1999; Ilbert et al. 2006), which performs a simple χ^2 fitting method between the stellar population synthesis (SPS) theoretical models and data. Single burst models from Bruzual & Charlot (2003) and a Chabrier (2001) IMF are used. Models are redshifted using the photometric redshifts. We adopt the observed *ugri* magnitudes (and related 1σ uncertainties) within a 6 arcsec aperture of diameter, which are corrected for Galactic extinction using the map in Schlafly & Finkbeiner (2011). Total magnitudes derived from the Sérsic fitting, m_S, are used to correct the outcomes of LE PHARE for missing flux. The single burst assumption is suitable to describe the old stellar populations in the compact galaxies we are interested in Thomas et al. (2005) and Tortora et al. (2009). The estimated photometric ages are used to check if galaxies are compatible with being relic remnants of systems formed at $z \sim 2$. The degeneracy between age and metallicity in the stellar population analysis can be solved only with forthcoming spectroscopic follow-ups.

(v) *Galaxy classification.* Using LE PHARE, we have also fitted the observed magnitudes MAGAP_6 with a set of 66 empirical spectral templates used in Ilbert et al. (2006). The set is based on the four basic templates (Ell, Sbc, Scd, Irr) described in Coleman, Wu & Weedman (1980), and starburst models from Kinney et al. (1996). GISSEL synthetic models (Bruzual & Charlot 2003) are used to linearly extrapolate this set of templates into ultraviolet and near-infrared. The final set of 66 templates (22 for ellipticals, 17 for Sbc, 12 for Scd, 11 for Im and 4 for starburst) is obtained by linearly interpolating the original templates, in order to improve the sampling of the colour space. We have selected the ETGs by choosing the galaxies which are best fitted by one of the elliptical templates (see Napolitano et al., in preparation).

(vi) *Near-infrared photometry from VIKING-DR1.* As a complementary data set for our selection of compact galaxies, we have used the data from the first release (DR1) of the ESO VISTA Kilo Degree Infrared Galaxy (VIKING) survey. The VIKING survey is the KiDS twin survey, and provides the near-IR coverage of the same sky region in the five wavebands *Z*, *Y*, *J*, *H* and *Ks*. VIKING-DR1 consists of 108 observed tiles (Edge et al. 2013). We have found that it overlaps with ∼58 per cent of our 156 deg^2 in the KiDS survey. For uniformity, we have used photometry within the same aperture as the optical data: APERMAG_3 for VIKING and MAGAP_2 for KiDS, which correspond to an aperture of 2 arcsec of diameter. In particular, we have concentrated on *J* and *Ks* passbands, which we do not use for SPS fitting, but only to improve the star-galaxy separation criterion (Maddox et al. 2008; Muzzin et al. 2013) as will be discussed in details in the next section.

The sample of high-S/N galaxies is complete down to a magnitude of MAG_AUTO_r ∼ 21, which correspond to stellar masses $\gtrsim 5 \times 10^{10}$ up to redshift $z = 0.5$ (see see Napolitano et al., in preparation, for further details).

2.2 Selection of compact galaxies

MSCGs have been selected using the following criteria.

(i) *Massiveness*. The most massive galaxies with $M_\star > 8 \times 10^{10}\,M_\odot$ are taken (Trujillo et al. 2009), reducing the original sample of ∼380 000 galaxies to ∼30 600 massive galaxies.

(ii) *Compactness*. We select the densest galaxies by following recent literature (Trujillo et al. 2009). We get galaxies with median circularized radius, R_e, among the g, r and i bands, less than 1.5 kpc. About 1300 compact candidates remain after this selection.

(iii) *Best-fitting effective radii*. The best-fitting structural parameters are considered, taking those systems with a reduced χ^2_{2D} from 2DPHOT smaller than 1.5 in g, r and i filters (La Barbera et al. 2010). To avoid any accidental wrong fits we have also removed galaxies with unreasonable best-fitting parameters, applying a minimum value for the size ($R_e = 0.05$ arcsec), the Sérsic index ($n > 0.5$) and the axial ratio ($q = 0.1$) in all the bands. The minimum value in the Sérsic index has also allowed us to possibly remove misclassified stars, which are expected to be fitted by a box-like profile (mimicked by a Sérsic profile with $n \to 0$). These last criteria on the quality of the structural parameters reduce further the sample to the 106 highly reliable candidates.

(iv) *Eye-ball check*. We have made an eyeball inspection of the images and residuals from Sérsic fitting of the candidates, with the aim of removing problematic objects or possible misclassified stars. To reduce subjectivity, three of the authors have independently checked the images and graded them according to the following scheme: grade-2 are sure galaxies, grade-1 are uncertain galaxies lacking a well-defined elliptical shape, and grade-0 are misclassified objects (either stars or corrupted fits). The mean of the three classifications has been adopted as the final grade. In this way, we have retained those galaxies with a grade larger than 1, to include only systems graded by at least one of the observers as a sure galaxy. The candidates are further reduced to 96, after removing objects with significant contamination from neighbours.

(v) *Optical+NIR star-galaxy separation.* We have adopted a morphological criterion to perform the star-galaxy classification (Bertin & Arnouts 1996; La Barbera et al. 2008) and used visual inspection as ultimate check of the galaxy classification. However, based on optical data only a star can be still misclassified as a galaxy on the basis of its morphology, and this issue can be highly dramatic for very compact objects (generally with size comparable or smaller than the seeing). In absence of spectroscopic information, optical+NIR colour–colour diagrams can provide a strong constraint on the galaxy nature of the candidates (e.g. Maddox et al. 2008; Muzzin et al. 2013). In particular, g, J and Ks magnitudes within 2 arcsec of diameter are adopted for this purpose on those fields with coverage by the two surveys. The Vega VISTA magnitudes are converted to AB using the conversion formulae from LE PHARE, $J_{AB} = J_{Vega} + 0.930$ and $K_{AB} = K_{Vega} + 1.834$. Stars and galaxies with the best J and Ks photometry are also considered ($\delta J, \delta K < 0.05$). The results are shown in Fig. 1. Stars have blue $J - K$ colours (i.e. $J - K \lesssim 0.2$, see light blue shaded region in Fig. 1). We have also found four objects with $J - K \lesssim 0.2$ and, indeed, are erroneously classified as galaxies. We take as compact candidates those systems with $J - K > 0.2$ and $g - J > 2$ (see light-yellow shaded region in Fig. 1). For those galaxies with available VIKING photometry, this selection allows our set of candidates from the previous classification steps to be refined. Out of 46 galaxies with VIKING photometry, we remain with 42 high-confidence candidates.

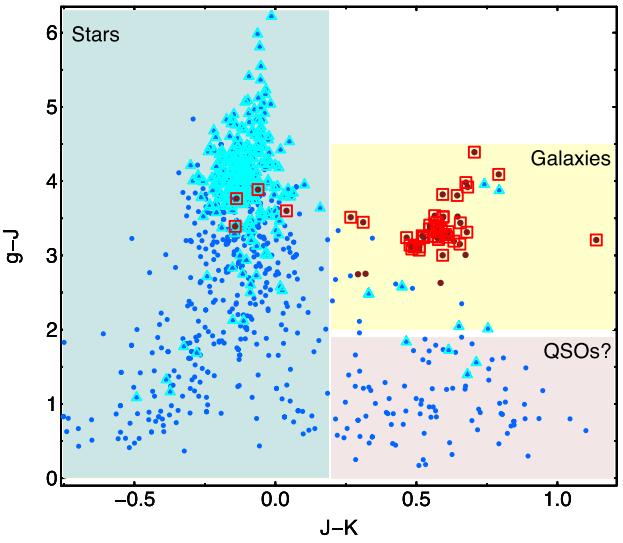

Figure 1. $J - K$ versus $g - J$ diagram. An aperture of 2 arcsec of diameter is adopted here. Blue and cyan symbols are for high-confidence stars with any error and $\delta J = \delta K < 0.05$, respectively. Red points and open boxes are for compact candidates with any error and $\delta J = \delta K < 0.05$, survived after the criteria on the mass, size, 2D fit quality and visual inspection. Vega J and K magnitudes are converted to AB as $J_{AB} = J_{Vega} + 0.930$ and $K_{AB} = K_{Vega} + 1.834$. We highlight the regions which are populated by stars (blue), galaxies (yellow) and QSOs (pink). We have considered as sure galaxies those objects with colours $J - K > 0.2$ and $g - j > 2$ (yellow shaded region).

In Fig. 1 we have also highlighted the locus populated by point sources with red $J - K$ ($\gtrsim 0.2$), but blue $g - J$ ($\lesssim 2$) colours, classified as stars by SExtractor, which are presumably quasars (Maddox et al. 2008, see pink region in Fig. 1). However, the analysis of this class of objects is beyond the scope of the paper.

To perform an homogeneous comparison of the sample of our compact candidates with a sample of 'normal' galaxies, using the same original catalogue described in Section 2, we have created two control samples (C-Samples) of galaxies with similar stellar masses ($M_\star > 8 \times 10^{10}\,M_\odot$), the same lower limits on Sérsic index ($n > 0.5$), axis ratio ($q > 0.1$) and R_e ($R_e > 0.05$ arcsec) as those for the compact systems, but without applying any compactness criterion. The first FULL C-Sample consists of all galaxies, with no restriction on the galaxy type, while the ETGs C-Sample consists of ETGs, classified as described in Section 2.

3 RESULTS

3.1 The final sample

We start by summarizing the sample we are left with for our analysis: after the first three criteria we have selected 106 candidates, which are reduced to 96 after the eye-ball check in (iv). The matching with VIKING included 46 candidates and, after applying the criterion (v), we are left with a sample of 42 out 46 galaxy candidates (i.e. 4/46 objects are likely stars according to their optical-NIR colours, corresponding to a ∼10 per cent contamination). Updating the total number, we are left with 92 candidates, of which ∼4 further sources from the region that does not overlap with VIKING might be stars. This corresponds to a density of ∼0.9 compact galaxies per square degree, cumulatively for $z \lesssim 0.7$, while we do not find objects at $z \lesssim 0.2$. In contrast, Trujillo et al. (2009) find 29 secure MSCGs at $z < 0.2$

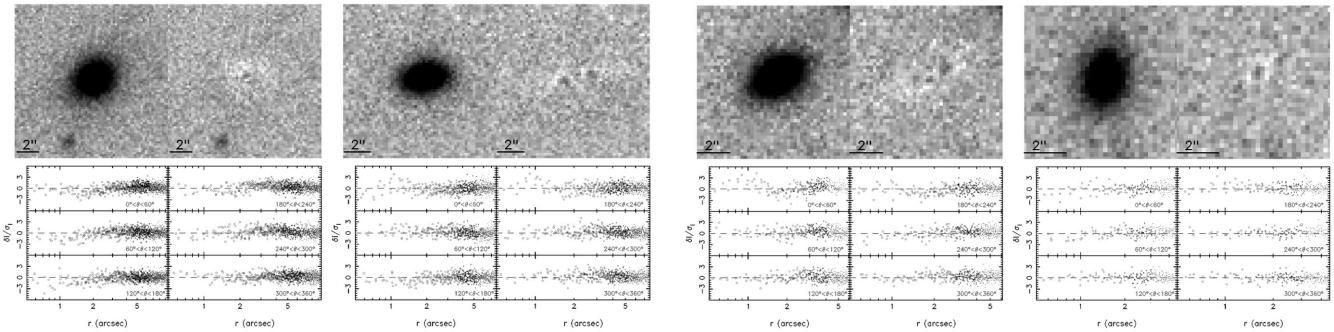

Figure 2. 2D fit output for four example candidates from 2DPHOT procedure. For each galaxy, the top panels show the galaxy image (left) and the residual after the fit (right), while the six bottom panels provide residuals after subtraction, plotted as a function of the distance to the galaxy centre, with each panel corresponding to a different bin of the polar angle. Residuals are normalized with the noise expected from the model in each pixel.

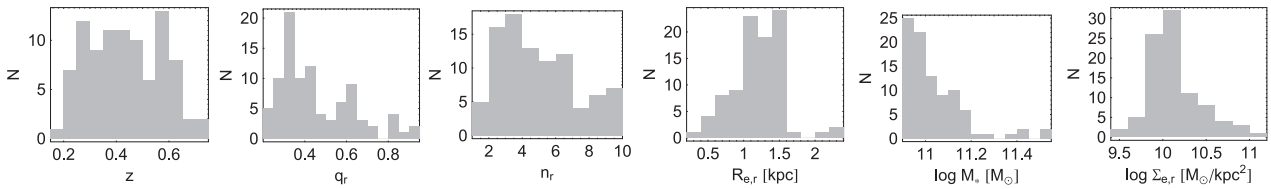

Figure 3. Distribution of some galaxy parameters. From left to right we show: (1) photometric redshifts, (2) *r*-band axis ratio, (3) *r*-band Sérsic index, (4) *r*-band effective radius, (5) Chabrier IMF-based stellar mass, (6) *r*-band effective surface mass density.

within the SDSS area, using our same criteria. However, only one of these is at very low redshift ($z < 0.1$), and none of them features old stellar populations (Ferré-Mateu et al. 2012), and thus they cannot actually be classified as relics. The absence of compact systems at $z < 0.2$ in our data sample might be related to environmental issues, since in the current KiDS area we are missing nearby clusters of galaxies, where a larger fraction of compact galaxies is predicted (Stringer et al. 2015), and seems to be observed indeed (Valentinuzzi et al. 2010; Poggianti et al. 2013a). A similar environment effect would be present in the Trujillo et al. (2009) sample. Examples of the 2D fitting results for four candidates are presented in Fig. 2, where postage stamps of the galaxy images and the residuals are shown.

Fig. 3 shows the distributions of redshift, axis ratio, Sérsic index, effective radius, stellar mass and surface mass density for our sample of compact candidates. The median redshift of the sample is ∼0.44, with an rms of ∼0.18, larger than the median redshifts of the FULL and ETGs C-Samples (∼0.36 and ∼0.34, respectively). Compact candidates have a median *r*-band effective radius of ∼1.2 kpc (rms = 0.31 kpc), a Sérsic index of ∼4.3 (rms = 2.3), an axis ratio of 0.40 (rms = 0.14) and median stellar mass of ∼10.99 dex (rms = 0.09). On the contrary, for the FULL C-Sample the median size, Sérsic index, axis ratio and $M_\star$ are ∼7.7 kpc, 4.7, 0.73 and ∼11.07 dex, respectively. Finally, if the ETGs C-Sample is considered, the median size, Sérsic index, axis ratio and $M_\star$ are ∼8.4 kpc, 5.5, 0.75 and ∼11.10 dex, respectively. Thus, smaller sizes translate into shallower light profiles (smaller *n*) when compacts are compared with normal galaxies (consistently with the galaxy merging framework in Hilz et al. 2013). Compact candidates also present lower axis ratios than normal galaxies. These elongated shapes are common in massive compact galaxies, both at high-*z* (van der Wel et al. 2011; Buitrago et al. 2013), and at lower redshifts (Trujillo et al. 2012, 2014).

In our compact sample, the average surface mass density within 1 R_e is $\sim 1.2 \times 10^{10}\,M_\odot\,kpc^{-2}$ (rms of $\sim 5.6 \times 10^9\,M_\odot\,kpc^{-2}$), about 2 orders of magnitude larger than the average surface mass density

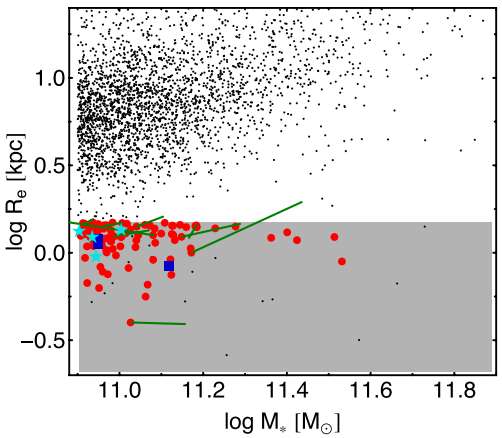

Figure 4. We show the median of the R_e in the *g*, *r* and *i* bands versus stellar mass. Compact candidates (plotted as red points) are compared with a selection of galaxies (∼2500 randomly extracted) from the FULL C-Sample (small black points). Grey shaded region highlight the region where candidates are selected (see text for details about the adopted selection criteria). We also plot the change if the spectroscopic redshift is used (dark-green lines). Finally, the four compact galaxies with $z < 0.2$ from Trujillo et al. (2012) and the three compacts at $z \sim 2$ from Szomoru et al. (2012), that fulfil our selection criteria, are shown as cyan stars and blue squares, respectively.

of the C-Samples. This median density is a bit larger than the range of values of 7–15 $\times\ 10^9\,M_\odot\,kpc^{-2}$ found in four compact galaxies at $z < 0.2$ by Trujillo et al. (2012), but the values are consistent within the scatter. Taking the only three galaxies from Szomoru, Franx & van Dokkum (2012), which satisfy the same criteria we are adopting in this paper, we find a median density of $\sim 1.1 \times 10^{10}\,M_\odot\,kpc^{-2}$, which is fully consistent with our result.

The *r*-band R_e as a function of $M_\star$ is shown in Fig. 4. The compact candidates are plotted with a random subset of ∼2500 galaxies from the FULL C-Sample. As the compact candidates are selected to

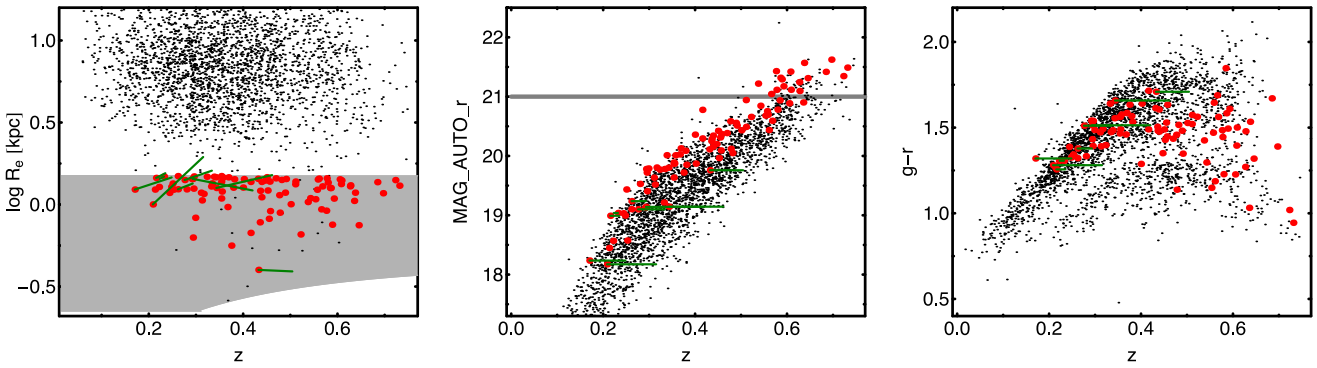

Figure 5. We show the median of the R_e in the g, r and i bands (left), r-band MAG_AUTO (middle) and $g - r$ (right) versus redshift. The grey region in the left-hand panel sets the region within which we have searched the compacts. Grey line in the middle panel sets the 90 per cent completeness limit of the high–S/N sample. The $g - r$ colour is calculated within 6 arcsec of diameter. See further details about the symbols in Fig. 4.

have small sizes, they lie in a region of the size–mass diagram where very few objects are detected, which provides a further evidence in favour of the rarity of these compact objects at $z \lesssim 0.7$ (Fig. 4; Trujillo et al. 2009). In Fig. 4 we also overplot the $z < 0.2$ galaxies in Trujillo et al. (2012) and the three $z \sim 2$ galaxies in Szomoru et al. (2012) which fulfil our selection criteria. The evolution with redshift of the sizes, magnitudes and colours are shown in Fig. 5. The R_es look quite constant as a function of redshift for the compact systems. At all the redshifts, almost all the compacts have faint MAG_AUTO when compared with the control sample population (middle panel in Fig. 5). We find that 75 candidates (∼82 per cent of the whole sample) lie below the r-band magnitude completeness limit of ∼21, implying that our sample is complete up to redshift $z \sim 0.5$. Finally, most of the galaxies populate the red-sequence, and are the best candidates to be remnants of high-z red nuggets (right-hand panel in Fig. 5).

58 out of 92 galaxies have old ages consistent with a formation redshift $z_f \gtrsim 2$, and so could be the remnants of the compact galaxies observed at $z > 1$ (Gargiulo, Saracco & Longhetti 2011; Gargiulo et al. 2012; Szomoru et al. 2012). 82 out of 92 galaxies (i.e. ∼89 per cent of the whole sample) are best fitted by an elliptical template, and are classified as ETGs (see Section 2). The rest of the galaxies have redshifts $z > 0.5$ and have colours which are best fitted by Sbc models. However, particularly at these redshifts, one should take this colour-based classification with caution, as a spectroscopic follow-up is actually needed to perform an accurate stellar population analysis.

3.2 Systematics from wrong redshifts

We have finally cross-matched our sample of candidates with SDSS and GAMA spectroscopy catalogues, finding spectra for nine of the selected candidates.

One of the main systematics in our selection of compact galaxies is induced by wrong redshift determinations, which can affect both the (linear) effective radii and stellar masses, moving the compact out of our selection criteria (e.g. see Figs 4 and 5). Seven out nine of these systems are included in the SDSS+GAMA datasample used for photometric redshift determinations (see Section 2): five in the training sample and two in the test sample. Although the photometric redshifts are shown to approximate quite well the spectroscopic ones (see Section 2 and Cavuoti et al. 2015), we note that almost all of the photometric redshifts are underestimated with respect to the spectroscopic value. The median difference $\Delta z \equiv z_{\rm phot} - z_{\rm spec}$ is −0.07, which increases to −0.1 if the galaxies not in the training sample are considered. This systematics can be probably related to the undersampling of this galaxy population, just five galaxies in the training sample, which can fail the optimum training of the network, and the quality of photometric redshift outcomes is degraded.

As first test, we have re-computed the sizes and stellar masses of these nine objects using the $z_{\rm spec}$. Only four galaxies survive to the size and mass selection criteria, i.e. ∼44 per cent (one not in the training sample).

Despite the small sample available for this test, we cannot exclude the presence of a systematics of the photometric redshift determination for compact sources which we might quantify of the order of $\Delta z = -0.1$. Qualitatively, if the spectroscopic redshift is larger than photometric one, then R_e in physical scale gets larger. The effect on $M_\star$ is not as simple as the one on R_e. As an exercise, we have investigated the impact of a redshift error of $\Delta z = 0.1$ on the 83 galaxies in the sample without spectroscopic redshift. Using re-calculated values for R_e and stellar mass, we find that 26 of the sources (31 per cent) survive the cuts.

Therefore, a spectroscopic follow-up will be needed to finally confirm the nature of these galaxies, allowing us to classify these candidates as compact or very compact galaxies. Increasing the knowledge base and the population of compact systems with measured spectroscopic redshifts will improve the quality of the photometric redshift estimates.

3.3 Colour gradients

A big improvement of our analysis with respect to previous works on compact galaxies at similar redshift ranges (e.g. Damjanov et al. 2014) is the high-S/N photometry which allows us to derive robust structural parameters and obtain the first determination of colour profiles for these systems. Therefore, following Tortora et al. (2010), we define the colour gradient as the angular coefficient of the relation $X - Y$ versus $\log R$, $\nabla_{X-Y} = \dfrac{\delta(X-Y)}{\delta \log R}$, measured in magdex^{-1} (omitted in the following unless needed for clarity). The fit of each colour profile is performed in the range $R_1 = 0.1 R_e \leq R \leq R_2 = R_e$, where the effective radius is measured in the r band. By definition, a positive CG, $\nabla_{X-Y} > 0$, means that a galaxy is redder as R increases, while it is bluer outward for a negative gradient. PSF-convolved Sérsic profiles in g, r and i band are used and, in particular, $g - r$, $r - i$ and $g - i$ colours are discussed. We omit detailed analysis in terms of redshift and stellar

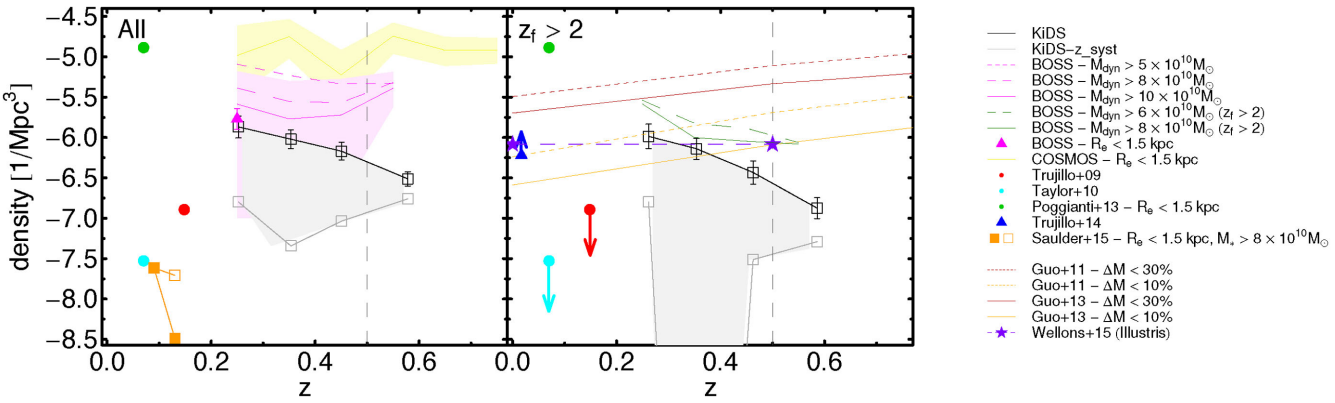

Figure 6. Number density of compact galaxies versus redshift. Error bars denote 1σ uncertainties (see the text). Vertical dashed black lines mark the completeness limit of the sample (see de Jong et al. 2015). Left. Number densities for all galaxies, independent of their photometric formation redshift, are plotted with open squares and solid black lines. The solid grey line with open squares takes into account possible systematics in the redshift determination (see Section 3.2). Short-dashed, long-dashed and solid violet lines are number densities of stellar-like objects from BOSS-DR10 (Damjanov et al. 2014) with $M_{\rm dyn} > 5 \times 10^{10}$, 8×10^{10} and 10^{11} $M_\odot$, respectively. The violet shaded region is the 1σ error for the case with $M_{\rm dyn} > 10^{11}$ $M_\odot$. The violet triangle with bars also shows the abundance of galaxies at $z \sim 0.25$, with $R_{\rm e} < 1.5$ kpc and $M_{\rm dyn} > 8 \times 10^{10}$ $M_\odot$, from Damjanov et al. (2014). The yellow line with lighter yellow region plot abundances for compacts in the COSMOS area (Damjanov et al. 2015a), selected with the same criteria as in this work ($M_\star > 8 \times 10^{10}$ $M_\odot$ and $R_{\rm e} < 1.5$ kpc; Damjanov, private communication). Red, cyan and green points are the results for compact galaxies from Trujillo et al. (2009), Taylor et al. (2010) and Poggianti et al. (2013a), respectively. Orange boxes show the abundances for compacts in SDSS area from Saulder et al. (2015), adopting our same criteria on mass and size. Filled boxes plot the results using Sérsic profiles, while open boxes are for the de Vaucouleurs profile (note that the results for the two profiles in the lowest redshift bin are superimposed). Right. Black open squares, solid lines and error bars plot KiDS number densities for candidate relic compacts, defined to have photometric formation redshift $z_f > 2$. Grey open squares and lines take into account possible systematics in the redshift determination. Long-dashed and solid green lines are for stellar-like objects from BOSS-DR10 with $z_f > 2$ (Damjanov et al. 2014) and $M_{\rm dyn} > 6 \times 10^{10}$ and 8×10^{10}, respectively. The results from Trujillo et al. (2009) and Taylor et al. (2010) are shown here as upper limits (see red and cyan points with arrows). The blue triangle is for the lower limit at $z \sim 0$ provided by Trujillo et al. (2014). Orange and red lines plot abundances of relic galaxies from SAMs, based on Millennium N-body simulations (Quilis & Trujillo 2013). Relics have been defined as systems whose stellar mass has increased since $z = 2$ to the present by less than 10 per cent and 30 per cent, respectively. Dashed and solid lines are for Guo et al. (2011a) and Guo et al. (2013) SAMs, respectively. Purple stars (connected by a line) are predictions from the Illustris simulations (Wellons et al. 2016).

mass, but we pinpoint what is the range of colour gradients in our galaxy sample, comparing these results with the `ETGs C-Sample` and some previous literature.

On average, compact population has $\nabla_{g-r} = -0.21$ (rms 0.52), $\nabla_{r-i} = -0.07$ (rms 0.59) and $\nabla_{g-i} = -0.30$ (rms 0.73) which are substantially consistent with the gradients for the control population of ETGs which are $\nabla_{g-r} = -0.17$ (rms 0.33), $\nabla_{r-i} = -0.05$ (rms 0.23) and $\nabla_{g-i} = -0.21$ (rms 0.40). Hence, compact candidates look quite similar to normal ETGs, except for the scatter, which is partially or totally related to the larger uncertainties on the structural parameters in our small objects.

These results agree with previously reported ranges of colour gradients of passively evolving massive galaxies at low- or intermediate-z (Tamura & Ohta 2000; Tamura et al. 2000; Wu et al. 2005; Tortora et al. 2010; La Barbera et al. 2012) or at high-z (Gargiulo et al. 2011, 2012; Guo et al. 2011b) and with simulations (e.g. Tortora et al. 2013).

Finally, we find that 30 compact candidates have all negative colour gradients, 9 have positive gradients, while the rest of the sample have at least one of the three gradients with a different sign with respect to the others. This wide range of behaviours demonstrate that these objects can be formed in quite different initial conditions (Gargiulo et al. 2012; Damjanov et al. 2014).

3.4 Abundance versus redshift

The number density of compact massive galaxies as a function of redshift is an important constraint on models of galaxy assembly. In recent years there have been different efforts to produce a census of such systems in different redshift bins (e.g. Trujillo et al. 2009; Taylor et al. 2010; Cassata et al. 2013; Poggianti et al. 2013a,b; Damjanov et al. 2014, 2015a; Saulder et al. 2015). Sample size is a crucial aspect to increase the constraining power. If the compact galaxies found in this work are a representative subsample of the whole population of compacts over the whole area of 1500 deg^2 that will be mapped by the KiDS survey, we expect to increase the present sample by a factor of 10 in the next few years.

For what concerns our current sample, we have binned galaxies with respect to redshift and normalized to the comoving volume corresponding to the observed KiDS sky area.[1] The errors on number counts take into account fluctuations due to Poisson noise, as well as those due to large-scale structure (i.e. the cosmic variance): they are calculated with the online `CosmicVarianceCalculator`[2] tool (Trenti & Stiavelli 2008). The cosmic variance increases the Poissonian error budget by ∼5–30 per cent. The total relative error on abundances (i.e. number densities) amounts to ∼25–30 per cent.

In Fig. 6 we plot the redshift evolution of the abundance of compact galaxies (left-hand panel) and that for the subsample of systems with old photometric ages (i.e. formation redshift $z_f \geq 2$; right-hand panel). We consider these potentially old `MSCGs`, as candidate remnants of the compact ETGs found at high redshift by several studies (see Section 1). We also re-determine the abundances by accounting for possible systematics in the photometric redshifts

[1] This is obtained by multiplying the number of candidates by $f_{\rm area} = A_{\rm sky}/A_{\rm survey}$, where $A_{\rm sky}$ (=41 253 deg^2) is the full sky area and $A_{\rm survey}$ = 105.4 is the effective KiDS-DR2 area. Then, the density is derived by dividing for the comoving volume corresponding to each redshift bin.
[2] http://casa.colorado.edu/~trenti/CosmicVariance.html

(see Section 3.2; see grey symbols in Fig. 6). We remind the reader that our sample starts to be incomplete at $z \gtrsim 0.5$ (see vertical dashed lines).

In the left-hand panel of Fig. 6, we plot number densities for the whole sample of KiDS compacts, independent of the galaxy formation redshift. Our number densities are compared with estimates from Damjanov et al. (2014), for the number density of stellar-like objects having spectroscopic redshifts from BOSS-DR10 (Ahn et al. 2014) and with three different cuts in total dynamical mass, $M_{\rm dyn}$ ($>5 \times 10^{10}$, 8×10^{10} and 10^{11} $M_\odot$, respectively; see Fig. 6). Notice that objects in the Damjanov et al. (2014) sample are not classified according to either morphology or galaxy age, nor do they have an accurate estimate of the intrinsic $R_{\rm e}$. Hence, their selection may be missing compact systems that are actually spatially resolved in BOSS-DR10. On the other hand, since Damjanov et al. (2014) also include compacts with $R_{\rm e} > 1.5$ kpc and are selected with respect to $M_{\rm dyn}$, rather than $M_\star$, it is not surprising, perhaps, that those abundance estimates are larger than ours. In fact, if we consider the abundance estimate of massive BOSS targets with $R_{\rm e} < 1.5$ kpc and $M_{\rm dyn} > 8 \times 10^{10}$ $M_\odot$ from Damjanov et al. (2014) (see purple triangle in the left-hand panel of Fig. 6), the number density of compacts in the lowest redshift bin ($z \sim 0.25$) is $(1.7 \pm 0.5) \times 10^{-6}$ Mpc^{-3}, in much better agreement with our density estimate of $(1.6 \pm 0.4) \times 10^{-6}$ Mpc^{-3} for the same redshift bin. On the other hand, selecting galaxies with $R_{\rm e} < 2.5$ kpc in KiDS, would lead to abundances $\sim$0.8 dex larger than for $R_{\rm e} < 1.5$ kpc, still in good agreement with estimates for stellar-like objects from Damjanov et al. (2014). The yellow region in the left-hand panel of Fig. 6 plots number densities for galaxies in the COSMOS survey (Damjanov et al. 2015a).[3] Remarkably, no evolution with redshift is found, for both KiDS and COSMOS samples, although, surprisingly, abundances for COSMOS (on average $\sim 10^{-5}$ Mpc^{-3}) are about one order of magnitude larger than our KiDS estimates. Since Damjanov et al. (2014) claim to find consistent density estimates between COSMOS and BOSS (the latter having an area 4000 times larger than COSMOS), cosmic variance seems not to be responsible for the above discrepancy. However, we cannot exclude that galaxy environment, which might be the actual driver of the number density of compact relics at $z \sim 0$ (see e.g. Valentinuzzi et al. 2010; Poggianti et al. 2013a; Trujillo et al. 2014), may be different for galaxies in the KiDS-DR2 and COSMOS areas – an issue that will be addressed in forthcoming extensions of this work.

The results for photometrically old MSCGs (right-hand panel of Fig. 6) are first compared with estimates for $z_f > 2$ compact galaxies from Damjanov et al. (2014), who selected samples with two cuts in $M_{\rm dyn}$ ($>6 \times 10^{10}$ and 8×10^{10}, respectively; see Fig. 6). As for the left-hand panel, there are differences in the selection criteria that make a direct comparison not trivial. However, the trends for both BOSS and KiDS samples look qualitatively similar, with a very mild evolution with redshift in the range where our KiDS sample is complete. Moreover, as noticed above, for BOSS compacts with $R_{\rm e} < 1.5$ kpc, the Damjanov et al. (2014) abundance estimates are fairly consistent with ours, within the uncertainties.

Finally, we compare MSCGs number densities with predictions from semi-analytical models[4] (SAMs). Quilis & Trujillo (2013) have determined the evolution of the abundance of compact galaxies from SAMs based on Millennium N-body simulations (Guo et al. 2011a, 2013), where relic compacts are defined as galaxies which have barely increased their stellar mass between $z \sim 2$ and $z \sim 0$. Operatively, they selected from the merger tree those objects that have increased their mass since $z = 2$ by less than 10 per cent and 30 per cent, respectively, i.e. galaxies whose mass at $z \sim 2$ is larger than 90 per cent and 70 per cent of the mass limit applied to select compacts. Our results are consistent in the lowest redshift bin with Guo et al. (2013) for simulated galaxies which have increased their mass at most by 10 per cent, while we estimate lower densities than in simulations at higher redshift. However, similarly to what discussed for the comparison to BOSS estimates, theoretical predictions should be actually considered as upper limits, as Quilis & Trujillo (2013) did not apply any precise selection in size, since the resolution in the simulations does not allow reliable estimates of galaxy effective radii to be obtained. We also compare our findings to results from the hydrodynamical Illustris simulation of Wellons et al. (2016) (see also Wellons et al. 2015). Wellons et al. (2016) select 35 massive and compact galaxies at $z = 2$ and follow their evolution to $z = 0$. Only 1 out of these 35 systems evolves into a galaxy that satisfies our mass and size criteria at $z \leq 0.5$. This corresponds to a number density of 8.28×10^{-7} Mpc^{-3}, which is consistent with the abundances of compact galaxies that have accreted less than 10 per cent of their final mass from the Millennium simulations. As a further caveat here, we point out that in our selection we adopt the same mass cutoff value at all redshifts, while simulations perform the mass selection at $z = 0$, implying that at high redshifts, simulated galaxies with masses smaller than the $z = 0$ cutoff value are actually included in the analysis. This is another reason why one may expect that predicted number densities for compacts at high redshift are actually higher than the observed ones.

At redshifts $z \lesssim 0.2$, in the left-hand panel of Fig. 6, we see a lack of candidates. This seems to contrast the results of Trujillo et al. (2009) who found 29 secure MSCGs at $z < 0.2$ fulfilling our same criteria, all of them having young ages $\lesssim$4 Gyr (see also Ferré-Mateu et al. 2012). However, one should notice that out of the 29 MSCGs of Trujillo et al. (2009), only one is at redshift <0.1, still pointing to the extreme paucity of such systems in the nearby Universe, consistent with our result. Similarly, Taylor et al. (2010) found one possible old MSCG at low redshift, using a more relaxed criterion for the size, than the one we adopt here.

Saulder et al. (2015) have found a sample of 76 compact galaxies from SDSS at $0.05 < z < 0.2$, which resemble quiescent galaxies at high-z, i.e. systems with small effective radii and large velocity dispersions. If we consider their compacts with $R_{\rm e} < 1.5$ kpc and $M_\star > 8 \times 10^{10}$ $M_\odot$, one galaxy at $z < 0.1$ and six galaxies at $z > 0.1$ are left when the effective radius from a de Vaucouleurs profile is used. Instead, these numbers change to one galaxy at $z < 0.1$ and only one at $z > 0.1$ if a Sérsic profile is fitted. These numbers correspond to abundances of 2.4×10^{-8} Mpc^{-3} in the redshift range $0.05 < z < 0.1$, and 2×10^{-8} Mpc^{-3} and 3.3×10^{-9} Mpc^{-3} at $0.1 < z < 0.2$, if de Vaucouleurs or Sérsic profile are fitted, respectively. As mentioned in Section 1, these findings seem to trouble the current hierarchical paradigm of galaxy formation, where some relic systems at $z \sim 0$ are actually expected to be found. In contrast, Poggianti et al. (2013a) have found four galaxies fulfilling our same criteria (corresponding to 1.4 per cent of their sample galaxies with masses larger than 8×10^{10} $M_\odot$), and all of these galaxies are old, with mass-weighted ages older than 8 Gyr. These numbers translate into a very large abundance of $\sim 10^{-5}$ Mpc^{-3}. Recently,

[3] These data are kindly computed for us by Damjanov (private comunication) by applying the same size and mass selection criteria as in this work.

[4] We caution the reader that stellar masses and sizes are measured in a different way between simulations and observations, hampering a straightforward comparison of the two.

Trujillo et al. (2014) added a new brick to the story, finding one relic compact in the Perseus cluster, i.e. NGC 1277, reconciling the observations at $z \lesssim 0.2$ with predictions from simulations. All these results point to an overabundance of MSCGs in dense cluster regions, that are actually under-represented over the area currently mapped by KiDS.

As discussed in Section 3.2, the sample of MSCGs would be reduced significantly in size by systematics in the redshift determination. Fig. 6 'corrects' the abundance estimates for the possible systematics in redshift. The corrected abundances (see grey boxes and lines in Fig. 6) should be seen as our current lower limit on number densities of SMCGs in KiDS. This issue will be addressed by on-going spectroscopic follow-up of MSCGs, and discussed in details in a future paper.

4 CONCLUSIONS

Thanks to the large area covered, high image quality, excellent spatial resolution and seeing, the KiDS provides a unique data set to study the properties of supercompact massive galaxies (MSCGs) – a family of systems which plays a key role into our understanding of galaxy formation and evolution.

In this paper, we present a sample of candidate MSCGs, based on 156 deg^2 of KiDS, in four optical bands (u, g, r and i). We start from a sample of ∼0.4 million galaxies with high S/N, measured photometry and structural parameters in all the four bands. For a subsample of these galaxies, we have used the KiDS photometry to estimate: (1) photometric redshifts based on machine learning techniques (Brescia et al. 2014; Cavuoti et al. 2015); (2) structural parameters using the software 2DPHOT (La Barbera et al. 2008); (3) stellar masses, fitting colours with SPS model predictions. The resulting sample is >90 per cent complete down to an r-band magnitude ∼21, and down to a stellar mass of 3–5 × 10^{10} $M_\odot$, up to a redshift $z \sim 0.5$. We select the most massive ($M_\star > 8 \times 10^{10}$) and most compact ($R_e < 1.5$ kpc) galaxies with (photometric) redshift $z \lesssim 0.7$. We remove star contaminants by performing a visual inspection of the final sample of candidates and then, for galaxies with available near-IR photometry from VIKING-DR1, we combine optical+NIR photometry to reduce the fraction of contaminants.

The final sample consists of 92 compact candidates, with a number density of ∼0.9 compact galaxies per square degree, at $z < 0.7$. Nine candidates have spectroscopic information from SDSS and GAMA surveys, that is used to assess the systematics in the redshift determination of our sample. On average, compact galaxies have negative colour gradients which are similar to the ones for normal passively evolving galaxies (e.g. Tamura & Ohta 2000; Tamura et al. 2000; Tortora et al. 2010, 2013; La Barbera et al. 2012). However, the variety of gradients, to be confirmed with a spectroscopic follow-up of the present sample, seems to suggest that compact galaxies formed under a wide range of initial conditions (Gargiulo et al. 2012). We also discuss the evolution with redshift of the number density of compact systems, and in particular that for the oldest galaxies, which are possibly remnants of the high-redshift ($z_f \gtrsim 2$) compact population detected by many studies. Remarkably, we do not find any MSCGs candidate at $z \lesssim 0.2$. This finding, which is consistent with the recent studies, might be related to the effect of galaxy environment on the abundance of compact systems (see Section 1). Although observational studies at intermediate- and high-z do not point to a clear picture of how environment affects galaxy sizes (see Damjanov et al. 2015b and references therein), recent cosmological simulations predict a larger fraction of massive compact systems in high- than in low-density regions (Stringer et al. 2015). This prediction is supported by the fact that NGC 1277 – the only well-characterized compact, massive, ETG at $z \sim 0$ – resides in the core region of a nearby rich cluster of galaxies (Trujillo et al. 2014; see also Valentinuzzi et al. 2010; Poggianti et al. 2013a). Thus, the absence of compact galaxies at $z < 0.2$ could be related to the smaller fraction of dense structures in the area currently mapped by KiDS.

We plan to have 10 times more compact candidates at the end of the KiDS survey, when all the 1500 deg^2 will have been observed. Only nine of our candidates have a spectroscopic coverage at the moment. Thus, a spectroscopic follow-up is actually necessary, to fully validate and characterize our sample, and determine accurate number densities to be compared with theoretical expectations.

ACKNOWLEDGEMENTS

Based on data products from observations made with ESO Telescopes at the La Silla Paranal Observatory under programme IDs 177.A-3016, 177.A-3017 and 177.A-3018, and on data products produced by Target/OmegaCEN, INAF-OACN, INAF-OAPD and the KiDS production team, on behalf of the KiDS consortium. OmegaCEN and the KiDS production team acknowledge support by NOVA and NWO-M grants. Members of INAF-OAPD and INAF-OACN also acknowledge the support from the Department of Physics & Astronomy of the University of Padova, and of the Department of Physics of Univ. Federico II (Naples). CT has received funding from the European Union Seventh Framework Programme (FP7/2007-2013) under grant agreement n. 267251 'Astronomy Fellowships in Italy' (AstroFIt). This work was partially funded by the MIUR PRIN Cosmology with Euclid. MB acknowledges the PRIN-INAF 2014 *Glittering kaleidoscopes in the sky: the multifaceted nature and role of Galaxy Clusters*. We thank the referee for his/her comments, which have helped to improve the paper. We thank I. Damjanov for having provided us with the abundances of compacts for the COSMOS field, applying the same size and mass selections as in this work. We thank M. Cacciato, R. C. E. Van den Bosch, M. Viola and I. Trujillo for helpful comments, B. Poggianti for comments about their findings at low redshift, V. Quilis who provided us with simulation predictions. We also thank S. Wellons and A. Pillepich for comments about their Illustris simulations.

REFERENCES

Ahn C. P. et al., 2012, ApJS, 203, 21
Ahn C. P. et al., 2014, ApJS, 211, 17
Arnouts S., Cristiani S., Moscardini L., Matarrese S., Lucchin F., Fontana A., Giallongo E., 1999, MNRAS, 310, 540
Belli S., Newman A. B., Ellis R. S., 2014, ApJ, 783, 117
Bertin E., Arnouts S., 1996, A&AS, 117, 393
Brescia M., Cavuoti S., D'Abrusco R., Longo G., Mercurio A., 2013, ApJ, 772, 140
Brescia M., Cavuoti S., Longo G., De Stefano V., 2014, A&A, 568, A126
Bruzual G., Charlot S., 2003, MNRAS, 344, 1000
Buitrago F., Trujillo I., Conselice C. J., Häußler B., 2013, MNRAS, 428, 1460
Capaccioli M., Schipani P., 2011, The Messenger, 146, 2
Cassata P. et al., 2013, ApJ, 775, 106
Cavuoti S. et al., 2015, MNRAS, 452, 3100
Chabrier G., 2001, ApJ, 554, 1274
Coleman G. D., Wu C.-C., Weedman D. W., 1980, ApJS, 43, 393
Daddi E. et al., 2005, ApJ, 626, 680
Damjanov I., Chilingarian I., Hwang H. S., Geller M. J., 2013, ApJ, 775, L48

Damjanov I., Hwang H. S., Geller M. J., Chilingarian I., 2014, ApJ, 793, 39
Damjanov I., Geller M. J., Zahid H. J., Hwang H. S., 2015a, ApJ, 806, 158
Damjanov I., Zahid H. J., Geller M. J., Hwang H. S., 2015b, ApJ, 815, 104
de Jong J. T. A. et al., 2015, A&A, 582, A62
Dekel A., Burkert A., 2014, MNRAS, 438, 1870
Driver S. P. et al., 2011, MNRAS, 413, 971
Edge A., Sutherland W., Kuijken K., Driver S., McMahon R., Eales S., Emerson J. P., 2013, The Messenger, 154, 32
Fan L., Lapi A., De Zotti G., Danese L., 2008, ApJ, 689, L101
Fan L., Lapi A., Bressan A., Bernardi M., De Zotti G., Danese L., 2010, ApJ, 718, 1460
Ferré-Mateu A., Vazdekis A., Trujillo I., Sánchez-Blázquez P., Ricciardelli E., de la Rosa I. G., 2012, MNRAS, 423, 632
Ferré-Mateu A., Mezcua M., Trujillo I., Balcells M., van den Bosch R. C. E., 2015, ApJ, 808, 79
Gargiulo A., Saracco P., Longhetti M., 2011, MNRAS, 412, 1804
Gargiulo A., Saracco P., Longhetti M., La Barbera F., Tamburri S., 2012, MNRAS, 425, 2698
Genzel R. et al., 2008, ApJ, 687, 59
Guo Q. et al., 2011a, MNRAS, 413, 101
Guo Y. et al., 2011b, ApJ, 735, 18
Guo Q., White S., Angulo R. E., Henriques B., Lemson G., Boylan-Kolchin M., Thomas P., Short C., 2013, MNRAS, 428, 1351
Hilz M., Naab T., Ostriker J. P., 2013, MNRAS, 429, 2924
Hopkins P. F., Hernquist L., Cox T. J., Keres D., Wuyts S., 2009, ApJ, 691, 1424
Hopkins P. F. et al., 2010, ApJ, 724, 915
Hsu L.-Y., Stockton A., Shih H.-Y., 2014, ApJ, 796, 92
Ilbert O. et al., 2006, A&A, 457, 841
Khochfar S., Silk J., 2006, ApJ, 648, L21
Kinney A. L., Calzetti D., Bohlin R. C., McQuade K., Storchi-Bergmann T., Schmitt H. R., 1996, ApJ, 467, 38
Komatsu E. et al., 2011, ApJS, 192, 18
Kuijken K., 2011, The Messenger, 146, 8
Kuijken K. et al., 2004, in Moorwood A. F. M., Iye M., eds, Proc. SPIE Conf. Ser. Vol. 5492, Ground-based Instrumentation for Astronomy. SPIE, Bellingham, p. 484
La Barbera F., de Carvalho R. R., Kohl-Moreira J. L., Gal R. R., Soares-Santos M., Capaccioli M., Santos R., Sant'anna N., 2008, PASP, 120, 681
La Barbera F., de Carvalho R. R., de La Rosa I. G., Lopes P. A. A., Kohl-Moreira J. L., Capelato H. V., 2010, MNRAS, 408, 1313
La Barbera F., Ferreras I., de Carvalho R. R., Bruzual G., Charlot S., Pasquali A., Merlin E., 2012, MNRAS, 426, 2300
Läsker R., van den Bosch R. C. E., van de Ven G., Ferreras I., La Barbera F., Vazdekis A., Falcón-Barroso J., 2013, MNRAS, 434, L31
Maddox N., Hewett P. C., Warren S. J., Croom S. M., 2008, MNRAS, 386, 1605
Martín-Navarro I., La Barbera F., Vazdekis A., Ferré-Mateu A., Trujillo I., Beasley M. A., 2015, MNRAS, 451, 1081
Muzzin A. et al., 2013, ApJS, 206, 8
Poggianti B. M. et al., 2013a, ApJ, 762, 77
Poggianti B. M., Moretti A., Calvi R., D'Onofrio M., Valentinuzzi T., Fritz J., Renzini A., 2013b, ApJ, 777, 125
Quilis V., Trujillo I., 2013, ApJ, 773, L8
Saulder C., van den Bosch R. C. E., Mieske S., 2015, A&A, 578, A134
Schlafly E. F., Finkbeiner D. P., 2011, ApJ, 737, 103
Shih H.-Y., Stockton A., 2011, ApJ, 733, 45
Stockton A., Shih H.-Y., Larson K., Mann A. W., 2014, ApJ, 780, 134
Stringer M., Trujillo I., Dalla Vecchia C., Martinez-Valpuesta I., 2015, MNRAS, 449, 2396
Szomoru D., Franx M., van Dokkum P. G., 2012, ApJ, 749, 121
Tamura N., Ohta K., 2000, AJ, 120, 533
Tamura N., Kobayashi C., Arimoto N., Kodama T., Ohta K., 2000, AJ, 119, 2134
Taylor E. N., Franx M., Glazebrook K., Brinchmann J., van der Wel A., van Dokkum P. G., 2010, ApJ, 720, 723
Thomas D., Maraston C., Bender R., Mendes de Oliveira C., 2005, ApJ, 621, 673
Tortora C., Napolitano N. R., Romanowsky A. J., Capaccioli M., Covone G., 2009, MNRAS, 396, 1132
Tortora C., Napolitano N. R., Cardone V. F., Capaccioli M., Jetzer P., Molinaro R., 2010, MNRAS, 407, 144
Tortora C., Pipino A., D'Ercole A., Napolitano N. R., Matteucci F., 2013, MNRAS, 435, 786
Tortora C., Napolitano N. R., Saglia R. P., Romanowsky A. J., Covone G., Capaccioli M., 2014, MNRAS, 445, 162
Trenti M., Stiavelli M., 2008, ApJ, 676, 767
Trujillo I. et al., 2006, ApJ, 650, 18
Trujillo I., Conselice C. J., Bundy K., Cooper M. C., Eisenhardt P., Ellis R. S., 2007, MNRAS, 382, 109
Trujillo I., Cenarro A. J., de Lorenzo-Cáceres A., Vazdekis A., de la Rosa I. G., Cava A., 2009, ApJ, 692, L118
Trujillo I., Carrasco E. R., Ferré-Mateu A., 2012, ApJ, 751, 45
Trujillo I., Ferré-Mateu A., Balcells M., Vazdekis A., Sánchez-Blázquez P., 2014, ApJ, 780, L20
Valentinuzzi T. et al., 2010, ApJ, 712, 226
van der Wel A., Holden B. P., Zirm A. W., Franx M., Rettura A., Illingworth G. D., Ford H. C., 2008, ApJ, 688, 48
van der Wel A. et al., 2011, ApJ, 730, 38
van Dokkum P. G. et al., 2010, ApJ, 709, 1018
Wellons S. et al., 2015, MNRAS, 449, 361
Wellons S. et al., 2016, MNRAS, 456, 1030
Wu H., Shao Z., Mo H. J., Xia X., Deng Z., 2005, ApJ, 622, 244
Yildirim A., van den Bosch R. C. E., van de Ven G., Husemann B., Lyubenova M., Walsh J. L., Gebhardt K., Gültekin K., 2015, MNRAS, 452, 1792

This paper has been typeset from a TEX/LATEX file prepared by the author.